Raman characterization of semiconductors revisited

Fred H. Pollak

Physics Department, Brooklyn College of CUNY
Brooklyn, N.Y. 11210

and

Raphael Tsu

Energy Conversion Devices, Inc.
Troy, Michigan 48084

Abstract

We review a number of recent significant developments in the use of Raman scattering (first-order as well as second-order) to characterize semiconductors in bulk, thin film or device form. Areas to be discussed include microcrystalline and amorphous tetrahedrally bonded solids (particularly Si), ion-damage and laser-annealing effects, microscopic nature of potential fluctuations in alloy semiconductors (including single crystal metastable materials), determination of the composition dependence of conduction band effective mass and scattering times, HgCdTe and CdTe, zone-folding in superlattices, correlation of light scattering and transport properties in quantum well structures, interfaces (including semiconductor/vacuum, Schottky barriers, MOS, heterojunctions) and determination of strains (including temperature dependence) at the interface of Si on various substrates.

Introduction

Raman scattering (RS) is an extremely useful tool for characterizing semiconductors, either in bulk, thin film or device form. RS depends on electron-phonon (lattice vibrations) interactions[1,2] and therefore is an important complement to other spectroscopic techniques (ellipsometry, modulated reflectivity, luminescence, XPS, AES, LEED, SIMS, TEM) many of which are functions of the electronic states. Since electron-phonon interactions are very sensitive to local environments, RS can give information about material (or device) structure and/or quality on the scale of a few lattice constants. For example, this spectroscopic method can be used to study the microscopic nature of structural and/or compositional disorder, clustering, etc. Also since RS is a second order optical process[1,2] it contains symmetry information not available from first-order interactions. For example, in diamond and zincblende-type semiconductors first-order optical processes are not sensitive to the polarization of the radiation (relative to the crystal axes) whereas in RS the scattering intensity for a given phonon mode is a function of both the incident and scattered light polarizations. This dependence leads to symmetry information that can be utilized to characterize many materials parameters. Furthermore, by using various excitation lines with different penetration depths it is possible to perform depth profiling measurements.

In materials characterization RS has been used to evaluate such quantities as crystal quality, composition of alloy semiconductors, carrier concentration and scattering time ($n \gtrsim 10^{17}$ cm^{-3}), structural and compositional disorder, ion-damaged and laser-annealing effects, etc. These aspects of RS have been discussed in articles by Abstreiter et al[3] and Tsu.[4,5] RS can also be utilized to study the nature of oxides on compound semiconductors as discussed by G. Schwartz.[6] In this paper we review a number of recent significant developments in the use of Raman scattering (first-order as well as second-order) to characterize semiconductors in bulk, thin film or device form. Areas to be discussed include microcrystalline and amorphous tetrahedrally bonded solids (particularly Si), ion-damage and laser-annealing effects, microscopic nature of potential fluctuations in alloy semiconductors (including single crystal metastable materials), determination of the composition dependence of conduction band effective mass and scattering times, HgCdTe and CdTe, zone-folding in superlattices, correlation of light scattering and transport properties in quantum well structures, interfaces (including semiconductor/vacuum, Schottky barriers, MOS, heterojunctions) and determination of strains (including temperature dependence) at the interface of Si on various substrates.

Background of Raman Scattering

Raman spectroscopy involves two photons - one incident and one scattered - and hence is different from one photon processes.[1,2] In the Raman effect a photon is scattered inelastically by the solid with the subsequent creation or annihilation of a phonon.[7] The process is very similar to inelastic scattering of x-rays or neutrons by a crystal. The conservation rules (energy and momentum) for the first order Raman effect are:

$$\hbar\omega_s = \hbar\omega_i \pm \hbar\omega_p \tag{1}$$

$$\hbar\vec{k}_s = \hbar\vec{k}_i \pm \hbar\vec{q}_p \tag{2}$$

Table I. Symmetry selection rules for backscattering from "ideal" diamond - and-zincblende-type semiconductors

Mode \ Surface	< 100 >	< 110 >	< 111>
LO	Allowed a)	Forbidden	Allowed a)
TO	Forbidden	Allowed a)	Allowed a)

a) Allowed for this surface for at least one polarization configuration.

The second-order Raman effect is a scattering process in which two phonons participate [1]. They may both be created (giving a Stokes component in the scattered light) or one may be created and the other destroyed (giving a Stokes and anti-Stokes component) or both may be destroyed (giving an anti-Stokes component).

If the two created phonons have branch indices σ and σ' (e.g. TA, LA, etc.) and their wavevectors are q and q', then energy and momentum conservation give

$$\hbar\omega_{\sigma q} + \hbar\omega_{\sigma' q'} = \hbar\omega_i - \hbar\omega_s \tag{3}$$

$$\hbar\vec{q} + \hbar\vec{q}' = \hbar\vec{k}_i - \hbar\vec{k}_s \tag{4}$$

The branch indices and wavevectors can take all values consistent with these restrictions. Thus the wavevectors need not be small, as in first-order scattering, but can take on values throughout the Brillouin zone. The phonon wavevectors are typically three orders of magnitude larger than the light wavevectors over the major part of the zone, and Eq. (4) can be replaced by

$$\hbar\vec{q} + \hbar\vec{q}' = 0 \tag{5}$$

to a very good approximation. The vibrational frequencies are the same at wavevectors +q and -q, and the energy conservation condition can thus be written

$$\hbar\omega_{\sigma q} + \hbar\omega_{\sigma' q} = \hbar\omega_i - \hbar\omega_s \tag{6}$$

Amorphous and microcrystalline materials

Microcrystalline materials

The first-order Raman spectrum has provided a fast and convenient method to determine whether a semiconductor such as silicon is crystalline or amorphous. For example, as discussed above, the conservation of phonon momentum, q, in crystalline silicon (c-Si) leaves as Raman active only the zone center (q = 0) optic phonon at 522 cm^{-1} (see Fig. 1a), which gives rise to a single line with a natural linewidth of Γ_o = 3.5 cm^{-1}. In amorphous silicon (a-Si) the q-vector selection rule does not apply at all due to the loss of long range order. All phonons in Fig. 1a are therefore allowed and the Raman spectrum resembles the phonon density-of-states with prominent humps around 140 cm^{-1} and 480 cm^{-1}, the former having its origins in the TA phonon while the latter is related to the TO phonons [12]. Thus the observation of these broad features or the sharp line at 522 cm^{-1} has been used to differentiate between a-Si and c-Si.

Within the past several years a number of investigators have reported spectra intermediate between the two extreme cases described above [13]. They always involve a shift of the 522 cm^{-1} line towards lower energy accompanied by an asymmetric broadening. This phenomenon has been taken as

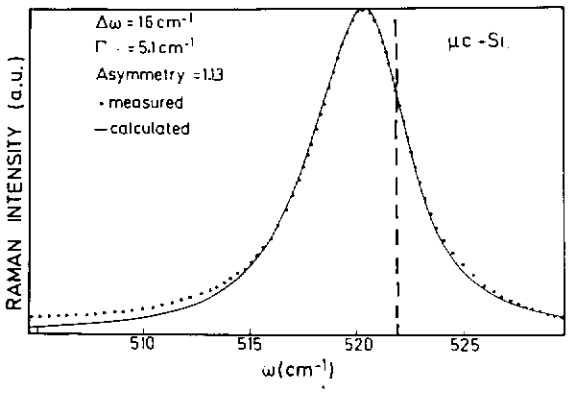

Fig. 2 Measured and calculated Raman line of a μc-Si sample. The dashed line indicates the Raman shift for c-Si. The asymmetry is defined as Γ_a/Γ_b where Γ_a and Γ_b are the low and high frequency half widths, respectively, of the Raman line (Ref. 13).

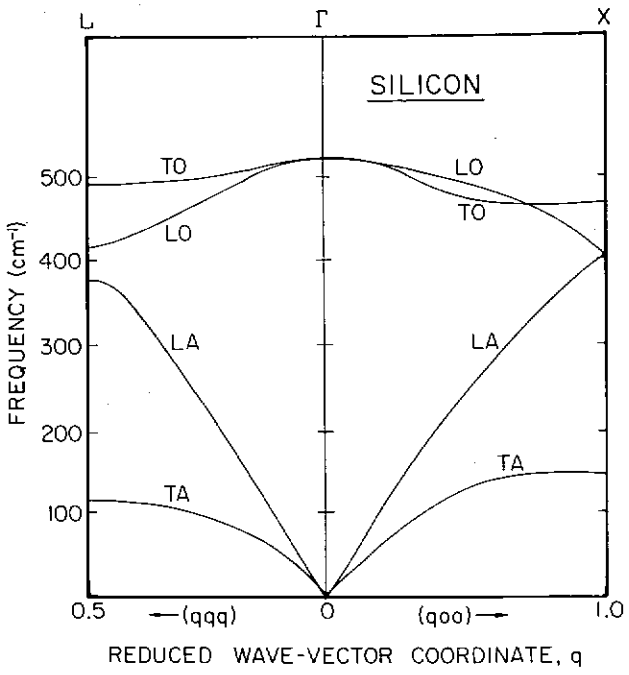

Fig. 1a Phonon dispersion curves along (100) and (111) for silicon.

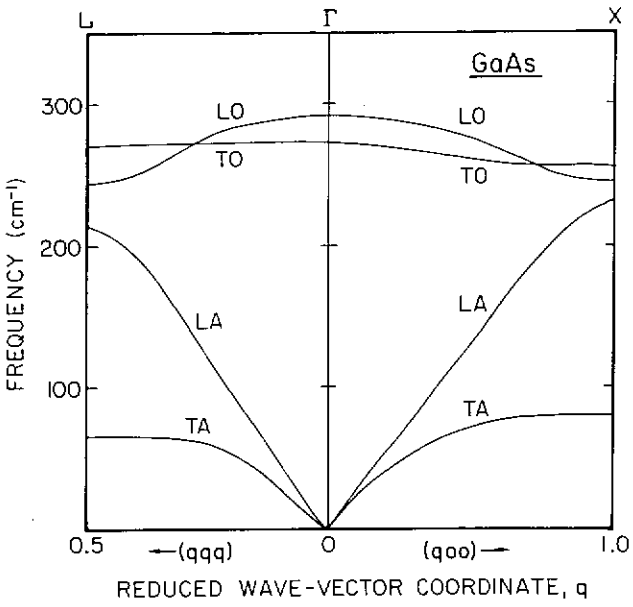

Fig. 1b Phonon dispersion curves along (100) and (111) for GaAs.

where $\hbar\omega_i$, $\hbar\vec{k}_i$ refer to the energy and momentum, respectively, of the incident photon, $\hbar\omega_s$, $\hbar\vec{k}_s$ refer to the scattered photon while $\hbar\omega_p$, $\hbar\vec{q}_p$ refer to the phonon created (minus sign) or destroyed (plus sign) in the scattering event. In Eqs. (1) and (2) the minus sign is called the Stokes component while the plus sign is the anti-Stokes component. Hence RS is a property of the vibrational modes of the semiconductor.

In an "ideal" crystal (i.e., a solid having translational symmetry) the spatial correlation (SC) length of the phonon is infinite[8] leading to plane-wave phonon eigenstates. Also the momentum of the incident light commonly used in RS (i.e., visible or near-visible lasers) is negligible compared with the crystal momentum. Thus the phonons involved in first-order RS have $\hbar q_p \simeq 0$ [see Eqs. (1) and (2)] and hence are at the center of the Brillouin zone (Γ- point). However, disorder or finite-size effects may partially or completely relax momentum conservation. In a material with structural disorder, the Raman spectrum is essentially that of the phonon density of states. Even in a material having only compositional disorder, momentum non-conserving processes may occur because of the potential fluctuations induced by a random distribution of different constituents.

Plotted in Fig. 1a and 1b are the phonon dispersion relations along < 100 > and < 111 > for the optic and acoustic phonons for Si and GaAs, respectively. For the diamond type material such as Si (which are homopolar) the q = 0 (Γ-point) optic phonons are triply degenerate and hence only one line is seen in the first order-Raman spectra of such solids. However, in the case of zincblende-type the q = 0 degeneracy is lifted because of the lack of inversion symmetry and the related polar character. The zone-center phonons are designated as longitudinal optic (LO) and transverse optic (TO) modes, the former always being at higher frequencies. Thus two features, LO and TO, are observed in the first-order RS of semiconductors such as GaAs. For many alloy semiconductors, such as $Ga_{1-x}Al_xAs$, a two-mode behavior is observed[3,4] i.e., GaAs-like and AlAs-like TO and LO phonons. It has been demonstrated that the internal fields associated with the LO phonon mode can couple to various collective electron modes.[3,4]

As discussed above the Raman intensity is a function of the polarization of the incident and scattered light relative to the crystal axes.[1,2] For example, in the backscattering configuration, which is employed in most semiconductors[9], only the LO phonon is allowed for the <100> surface, the TO mode being forbidden. However, for the case of the <110 > face the TO phonon is allowed while the LO mode is forbidden. For the <111> surface both LO and TO modes can be observed. These results are summarized in Table I. It should be pointed out that these selection rules are valid only for the "ideal" crystal, i.e., in the absence of perturbations (electric or magnetic fields, etc.) and/or q-linear terms.[10,11]

For the Group IV semiconductors these symmetry selection rules in general, have limited use since the LO and TO modes are degenerate. However, for zincblende type materials, since this degeneracy is removed, these selection rules can be employed to evaluate many important material parameters. For example, observation of the symmetry-forbidden TO mode from the < 100 > surface can be related to crystal quality.[4,5]

evidence of a " microcrystalline phase" in Si (μc-Si). A similar effect has been reported for μc-Ge[14] and μc-GaP [14].

Richter, Wang and Ley[13] have developed a detailed model to quantitatively explain this observation in silicon. A more qualitative model has been presented by Tsu et al [15]. For a finite material the mode correlation functions of the phonons become finite due to the lack of translational symmetry. Thus there is a relaxation of the q = 0 selection rules. Reference 13 has assumed a Gaussian localization factor exp $(-2r^2/L^2)$ for the phonon wave function, where L is the diameter of the microcrystalline phase (assumed to be spherical). Upon Fourier transformation this leads to an average over q with a similar weighting factor, exp $(-q^2L^2/4)$. The above considerations lead to a red shift and an asymmetric broadening with tailing towards low frequencies as the q = 0 selection rule is relaxed. Shown in Fig. 2 are the results of Ref. 13 with L = 40 Å for the μc-Si phase. The dashed line indicates the Raman shift for c-Si. The calculation produces a shift $\Delta\omega$ = 1.6 cm^{-1}, Γ = 5.1 cm^{-1} and an asymmetry = 1.13. The asymmetry is defined as Γ_a/Γ_b, where Γ_a and Γ_b are the low frequency and high frequency halfwidths, respectively, of the Raman line. The agreement between experiment and theory is quite good thus making it possible to evaluate the μc-Si particle size from the first-order Raman spectra.

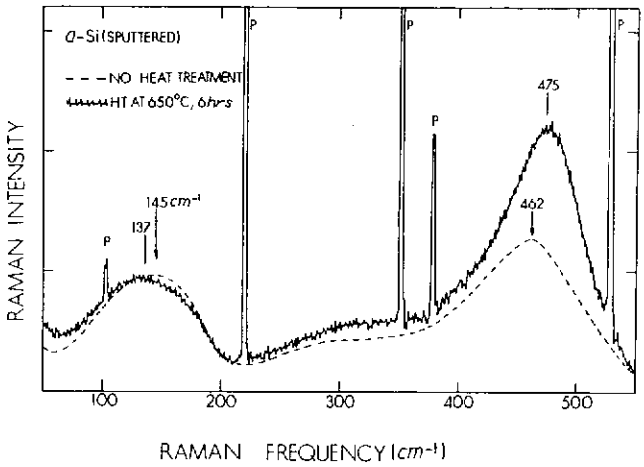

Fig. 3 Raman scattering intensity (in arbitrary units) vs. Raman frequencies (in cm^{-1}) for a sputtered sample before and after heat treatment at 650°C for 6 hours. The noise and plasma line for the sample before heating have been removed for clarity (Ref. 12).

We shall show below that the q-vector relaxation model can also be employed to explain the Raman spectra of topologically disorder semiconductors.

Structural and crystallization effects in a-Si, a-Ge and a-C

A number of investigators have used the features of the Raman spectra to gain insights into microscopic structural effects [12,16-23]. Tsu and co-workers have used the features of the Raman spectra of a-Si materials (a-SiF:H, a-SiH and sputtered a-Si) i.e. the broad features around 140 cm^{-1}(TA) and 480 cm^{-1} (TO) and the relatively sharp structure in the 500-522 cm^{-1} range (μc-Si phase) to investigate many important aspects of the growth and recrystallization of these solids [12,16].

For example, Raman scattering has been utilized to characterize the change in structural order parameter for three types of a-Si mentioned above. Figure 3 shows the Raman spectra for a sputtered a-Si sample before and after heat treatment [12]. The plasma lines of the Ar-ion laser (sharp features) were left in purposely to obtain an exact calibration of the Raman frequencies. Note that ω_{TO} shifts from 462 cm^{-1} before heat treatment to 475 cm^{-1} after annealing at 650°C for 6 hours while ω_{TA} shifts down from 145 to 137 cm^{-1}. There is also a very substantial change in the linewidth of the TO phonon and the intensity of the ratio I_{TO}/I_{TA}. Similar results for heat treated a-Si:F:H and a-Si:H. By correlating the Raman results with electronic properties, these authors were able to conclude from the above Raman features that in relation to a-Si (sputtered) there is an increase in local order in the amorphous phase for a-Si:H and particularly for a-Si:F:H. The improvement in structural order is consistent with the reduction in electronic gap states. These authors also have discussed the details of the Raman features, i.e. shifts, linewidths and intensities, in relation to topological and bond-angle variations [12].

Maley et al have used both Raman scattering and optical absorption measurements to investigate the substantial changes in a-Si deposited under conditions of variable substrate temperature [18]. These results indicate an approximately linear variation of the optical gap with the inverse width of the TO-like band. Also reported are similar preliminary results for a-Ge. These investigators mention that the variations in both the phonon and electronic states in these tetrahedrally coordinated amorphous solids are primarily due to modifications of the bond angle distribution.

Shimada et al studied the structural properties of the two phase silicon system (i.e., a-Si and μc-Si) by means of Raman scattering from the TA-like band [19]. They mention that this feature is a sensitive probe of the randomness of the Si-Si bonding structure in μc-Si.

Although the above articles have noted that a relation between bond-angle variation and Raman linewidth exists no detailed correlation has been made. Recently, a calculation [23] involving the experimental values of Raman-strain parameters of c-Si and c-Ge has been used to give a quantitative relation between the bond angle variations and the measured linewidth of the TO-like bands in a-Si and a-Ge, respectively.

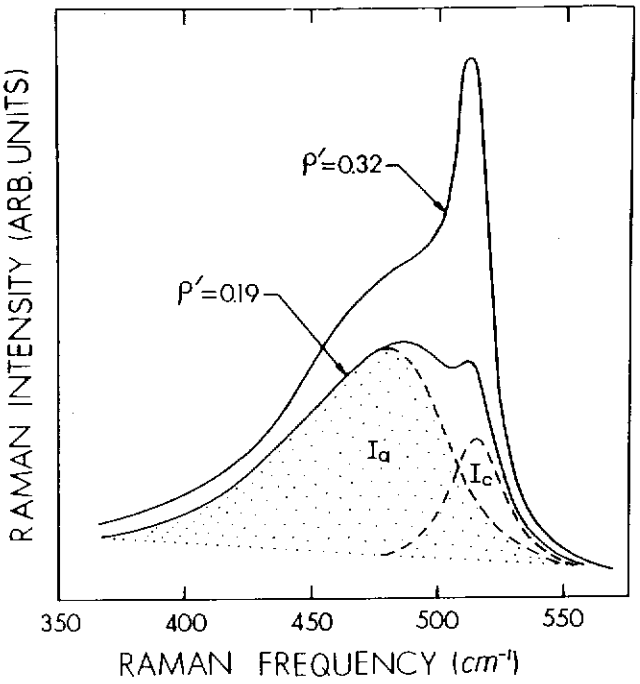

Fig. 4 Raman intensity versus Raman frequency for a two-phase system, microcrystallites embedded in an amorphous matrix (Ref. 17).

The details of the Raman spectra of the μc-Si phase (relatively sharp features in the 500-522 cm^{-1} range) have been employed to study the critical volume fraction for conductivity percolation in P-doped Si:F:H alloys[17] and the nucleation and growth rates of a-Si alloys [16]. In the former experiment a number of samples of highly P-doped a-Si:F:H alloys were prepared having a range of volume fraction, ρ, of c-Si embedded in an a-Si matrix. The integrated Raman scattering intensity I_c of the crystalline part relative to I_a of the amorphous component is used to deduce ρ. Figure 4 shows the typical Raman spectra of two such samples[17]

The curve denoted by $\rho' = 0.19$ has been resolved into two parts, I_a (shaded) and I_c. A computer program was used to fit a typical amorphous spectrum having a maximum located at 480 cm^{-1}. After subtracting I_a from the total measured scattering, the remaining area under the curve is attributed to I_c, the contribution of the fraction of crystallinity ρ. These authors have found that the measured critical volume fraction at the onset of rapidly increased conduction in this two-phase system of microcrystallites embedded in an amorphous matrix is $\rho_c = 0.18$. This value coincides with the theoretical percolation limit and serves to explain the conduction process in these two-phase materials.

Raman scattering has also been utilized to study amorphous and microcrystalline carbon and related materials such as graphite and coal[24]. Several studies show that as-deposited a-C films have only graphite-like bonding while annealing produces μc-C that grows in size with annealing conditions[20,21]. On the other hand a-C:H films prepared by glow discharge shows evidence for the μc-C phase with no annealing[22].

Ion-damage and laser annealing

Ion-damage and laser annealing in semiconductors are processes of considerable technological importance as well as methods of producing controlled damage for studying the nature of disorder in solids. There have been a number of studies utilizing Raman scattering to investigate ion-damage and laser annealing in diamond [5] and zincblende-type semiconductors [26].

Figure 5a shows the unpolarized backscattering Raman spectrum of an unimplanted sample of <100> GaAs (spectrum A). Indicated at the top of the figure are the positions of various zone center and zone edge phonons [25]. The prominent feature at 292 cm^{-1} in spectrum A is the LO phonon (q=0) with a natural linewidth of 3.0 cm^{-1}. The small feature at 269 cm^{-1} is the TO phonon (q=0) which is forbidden in the <100> backscattering geometry. The appearance of this peak was not due to misalignment since this experiment was performed in the true backscattering configuration. Tsu has discussed the origins of this feature in the forbidden configuration[4]. Also plotted in Fig. 5a are the spectra for a sample implanted with 270 keV As^+ ions to a fluence of 2.4 x 10^{13} cm^{-2} for various polarization configurations (spectra B, C, D and E). Spectrum F is that for material implanted to a fluence of 3.2 x 10^{14} cm^{-2}. The increasing fluence results in a continuous transformation of the Raman spectra from crystalline (spectrum A) to amorphous (spectrum F) material. Note also that for a fluence of 2.4 x 10^{13} cm^{-2} the polarization selection rule of the LO-phonon mode still are obeyed, i.e. it is allowed for the configuration of spectra B and C but is forbidden for the D and E geometries[1].

Plotted in Fig. 5b are the Raman features of a piece of undamaged semi-insulating (SI) GaAs (bottom spectrum), the SI GaAs implanted with Te^+ at 200 keV to a fluence of 5 x 10^{15} cm^2 (top spectrum) as well as the spectra of the implanted material that has been laser annealed with the 530 nm line of a Nd:YAG laser with 10n sec pulses at various power densities [4]. Note that the top spectra of Figs. 5a and 5b are quite similar, i.e. amorphous material with a broad peak at about 260 cm^{-1}. Annealing at 5 MW/cm^{-2} brings out two features at about 265 cm^{-1} (TO) and 285 cm^{-1} (LO). Note that the LO mode is asymmetric while the TO feature is relatively symmetric. With increased power density the LO mode gains in amplitude, shifts to higher frequencies, narrows and becomes more symmetric until at 40 MW/cm^2 it closely resembles the undamaged material. The TO mode decreases in amplitude (relative to the LO) and shifts only slightly to the blue. Thus the effects of laser annealing (Fig. 5b) are the inverse of ion-damage (Fig. 5a). In Fig. 6 is shown for 250-350 cm^{-1} the expanded version of the LO and symmetry-forbidden TO phonon for both the unimplanted and 2.4 x 10^{13} cm^{-2} implanted samples of Fig. 5a. The full width at half-maxima $\Gamma = (\Gamma_a + \Gamma_b)$ is indicated. Note that the LO phonon line for the implanted sample has (a) shifted to lower frequencies and (b) broadened asymmetrically ($\Gamma_a > \Gamma_b$). However, the TO feature shows only a small symmetrical

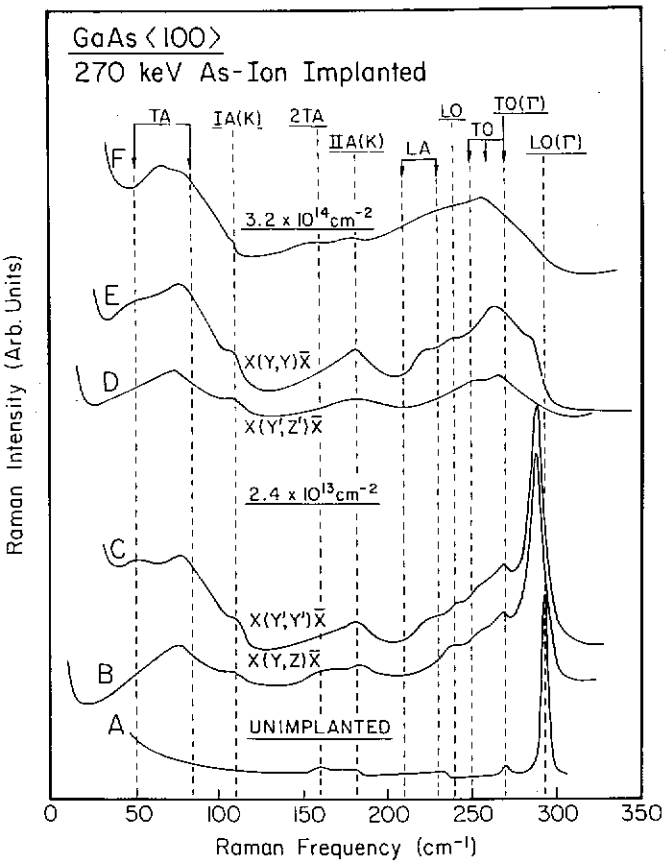

Fig. 5a Raman spectra of As-Ion implanted <100 > GaAs (Ref. 25).

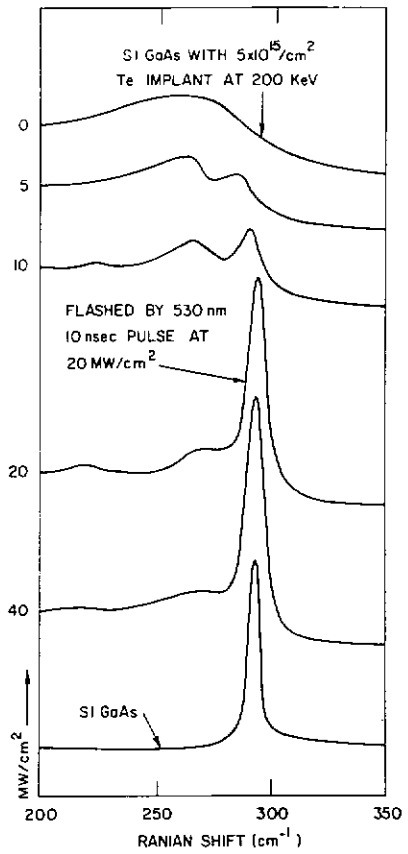

Fig. 5b Raman spectra of laser-annealed Te-implanted semi-insulating <100 > GaAs (Ref. 4).

red shift.

For the case of the ion-damaged material the behavior of the LO and TO modes has been quantitatively explained [25] in terms of a "spatial correlation" (SC) model similar to that used by Richter, Wang and Ley for μc-Si. As discussed before, in an "ideal" crystal the region over which the spatial correlation function of the phonon extends is infinite, thus leading to the usual phane-wave phonon eigenstates and the q=0 momentum selection rule of first-order Raman scattering. However, as the crystal is damaged by ion-bombardment the mode correlation functions become finite due to the induced defects. Thus, there is a relaxation of the q=0 selection rule and an associate finite "spatial correlation" size, L.

Based on these considerations it is possible to write $I(\omega)$, the Raman intensity at frequency ω, as:

$$I(\omega) \propto \int_0^1 \exp(-q^2L^2/4) \frac{d^3q}{\left[\omega - \omega(q)\right]^2 + \left[\Gamma_o/2\right]^2} \qquad (7)$$

where q is expressed in units of $2\pi/a$, a being the lattice constant. The parameter Γ_o (= 3.0 cm^{-1}) is the natural linewidth (full-width at half-maxima) of the undamaged material (having a Lorentzian lineshape) and $\omega(q)$ represents the dispersion relation of the phonon.

In order to calculate the Raman features of the LO phonon in ion-damaged GaAs, Ref. 25 employed Eq. (7) taking for the dispersion $\omega(q)$ the analytic model relationship:

$$\omega(q) = A + B\cos(\pi q) \qquad (8)$$

which with A = 269.5 cm^{-1} and B = 22.5 cm^{-1} reproduces quite well the dispersion of the LO phonon in GaAs (see Fig. 1b). Also a spherical Brillouin zone was assumed.

Figure 7 shows the shift $\Delta\omega_{LO}$ of the maximum of $I_{LO}(\omega)$ from 292 cm^{-1} and $\Gamma = \Gamma_a + \Gamma_b$, the full width at half maximum of the LO line as a function of L as evaluated from Eqs. (7) and (8) (solid line). Also shown are the experimental values of $\Delta\omega_{LO}$ and Γ for various fluences. From the above equations it is also possible to evaluate the asymmetry Γ_a/Γ_b in relation to ω_{LO} for various L. This is shown in

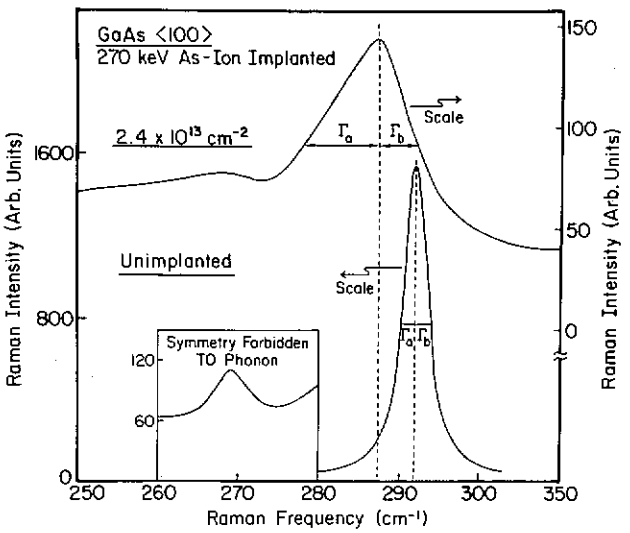

Fig. 6 Expanded version of spectra A and C of Fig. 5a in the range 250-350 cm^{-1} (Ref. 25).

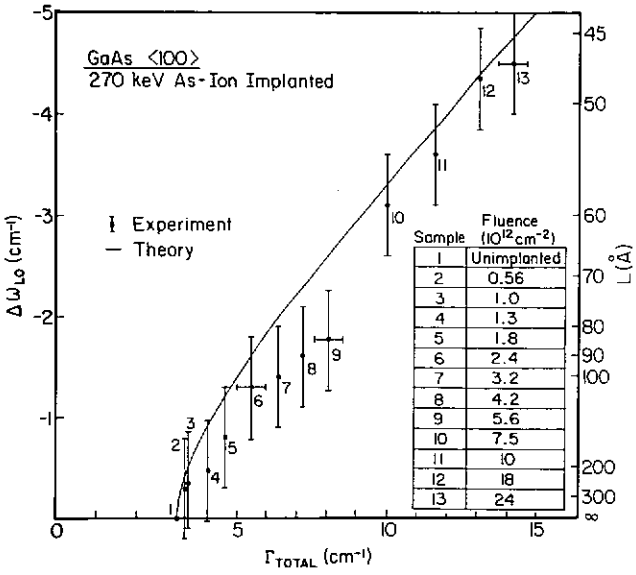

Fig. 7 The LO phonon shift, $\Delta\omega_{LO}$, and broadening, Γ as a function of L as determined from Eqs. (7) and (8)(solid line). Also shown are experimental points for various fluences (Ref. 25).

Fig. 8 together with the experimental values. The agreement in both cases is quite good. Thus from Figs. 7 and 8 it is possible to relate the shift, broadening and asymmetry of the LO phonon to an average undamaged particle size. For example, a fluence of 2.4×10^{13} cm^{-2} corresponds to an $L \approx 45$ Å. Such a relation between fluence and average undamaged region size is consistent with a recent scanning ellipsometry experiment performed on the same samples [27].

The SC model also explains the fact that the TO phonon exhibits only a small red shift. For this mode, in GaAs as in other III-V materials, there is little dispersion: ω_{TO} decreases by only about 10-15 cm^{-1} from zone center to the edge. Thus, for the TO phonon, A= 264 cm^{-1} and B= 6 cm^{-1} in Eq. (2). This dispersion, when substituted in Eq. (1), yields only a slight shift to lower frequencies with decreasing L down to about 45 Å. The evolution of zone-edge phonons with increasing fluence is a density-of-states effect that can also be understood on the basis of the SC model. From Eqs. (7) and (8), the intensity corresponding to the LO zone-edge phonon at 247 cm^{-1} is zero for large L but increases monotonically with decreasing L.

For ion-damaged GaP Myers et al. [26] have also observed with first-order Raman spectra a softening and asymmetric broadening of the LO phonon and almost no shift of the TO mode. These results are interpreted in terms of the disruption of the long-range ionic ordering which weakens the Coulomb interaction that is responsible for the difference in energy between the long-wavelength LO and TO phonons. Thus, in their model, the reduction of the coherence length of the LO mode shifts its energy back to that of the TO phonon as the damage increases. Such an interpretation explains qualitatively the softening and asymmetric broadening of the LO phonon line and the relative stability of the TO mode. There appears to be no contradiction between the approach of Ref. 25 and that of Ref. 26 since both rely on the concept of the reduction in coherence length of the phonon modes. The above analysis is also consistent with the suggestion of Nakamura and Katoda [28] that

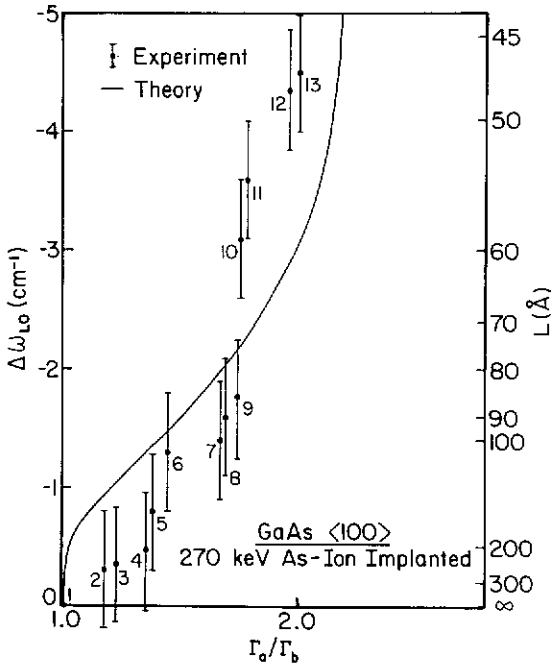

Fig. 8 The LO phonon shift, $\Delta\omega_{LO}$, and asymmetry, Γ_a/Γ_b, as a function of L is determined from Eqs. (7) and (8) (solid line). Also shown are experimental points for various fluences (Ref. 25).

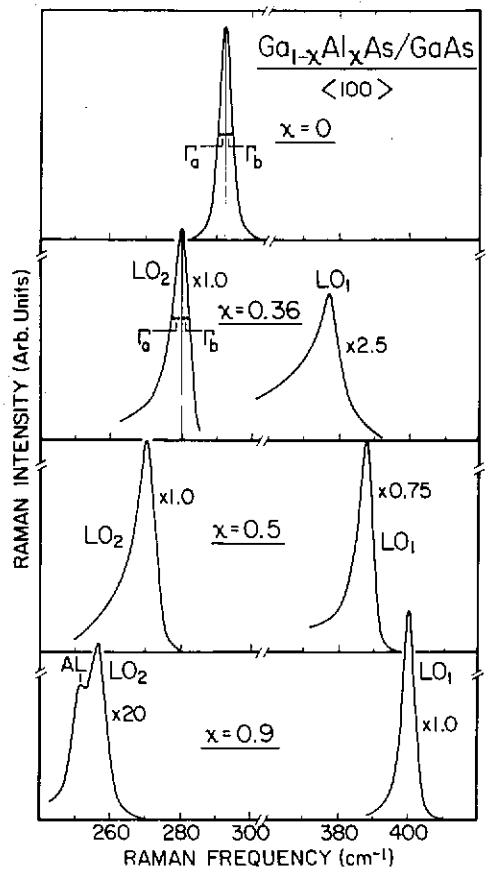

Fig. 9 Raman spectra of the LO phonons from several < 100> $Ga_{1-x}Al_xAs/GaAs$ samples for x =0, 0.36, 0.5, 0.9 (Ref. 31).

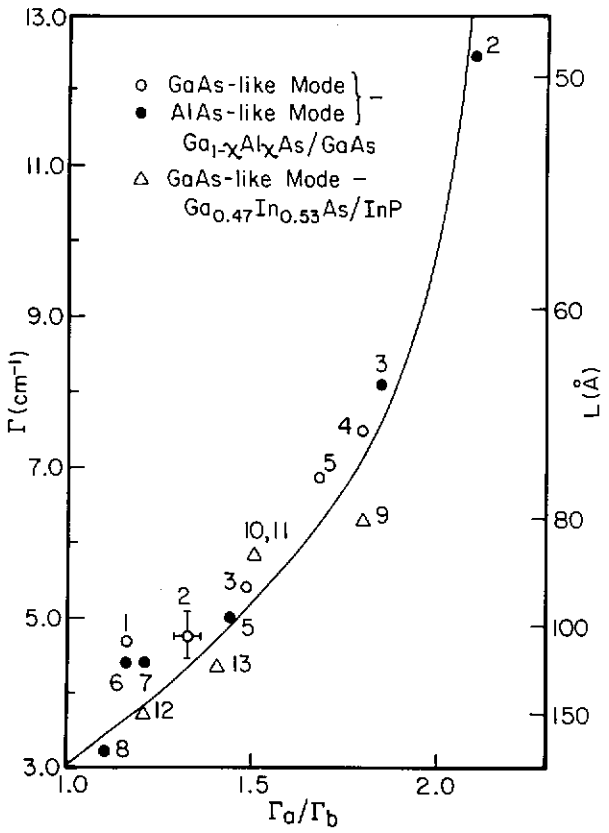

Fig. 10 Broadening, Γ , and asymmetry, Γ_a / Γ_b , of the LO phonon as a function of L from Eqs. (7) and (8) (solid line). Also shown are experimental points for a number of $Ga_{1-x}Al_xAs/GaAs$ and $Ga_{0.47}In_{0.53}As/InP$ samples. Representative error bars are shown (Ref. 31). The characteristics of the samples are listed in Table II.

their implanted samples contain partly crystallized regions.

Alloy semiconductors

Alloy potential fluctuations

In an alloy semiconductor such as $Ga_{1-x}Al_xAs$ there exist potential fluctuations due to the microscopic nature of the compositional disorder and hence translational invariance is broken. This effect also will manifest itself as a q-vector relaxation process. Indeed, it is found that in ternary alloy semiconductors the LO phonon mode is asymmetric ($\Gamma_a > \Gamma_b$) and broader than that of the binary end point materials[3,4,29,30].

First-order Raman scattering Shown in Fig. 9 are the LO phonon spectra from the <100> surface of $Ga_{1-x}Al_xAs$ for x=0, 0.39, 0.5 and 0.9. This material exhibits a two-mode behavior i.e., AlAs-like (LO_1) and GaAs-like (LO_2) features for $0 < x < 1$. The GaAs LO-mode (x=0) has a symmetric lineshape with Γ_o=3 cm^{-1} while the other spectra are asymmetric ($\Gamma_a > \Gamma_b$) with a total linewidth Γ greater than that of GaAs. For the x=0.9 material the lineshape of LO_2 is complicated by the presence of the AL feature, which has been ascribed to localized phonon mode due to the motion of As atoms about a Ga atom on an Al site[4]. The behavior of the alloy spectra, i.e., broadening and asymmetry also can be quantitatively accounted for by q - vector relaxation induced by the microscopic nature of the alloy potential fluctuations[31]. In this case the variable L can be thought of as a correlation length over which the material is compositionally ordered.

Plotted as the solid line in Fig. 10 is the broadening Γ and asymmetry Γ_a / Γ_b as a function of the correlation length L as determined from Eqs. (7) and (8). Also plotted in this figure are the experimental points for the GaAs-like and AlAs-like modes of a number of samples of $Ga_{1-x}Al_xAs/GaAs$ (the data for sample #4 is taken from Ref. 32) as well as the GaAs-like mode of $Ga_{0.47}In_{0.53}As/InP$ [for this material the

Table II. Characteristics of the $Ga_{1-x}Al_xAs/GaAs$ and $Ga_{0.47}In_{0.53}As/InP$ samples in Fig. 10.

Sample	Material	Growth Technique
1	$Ga_{0.79}Al_{0.21}As/GaAs$	MOCVD
2	$Ga_{0.64}Al_{0.36}As/GaAs$	MBE
3	$Ga_{0.6}Al_{0.4}As/GaAs$	MBE
4	$Ga_{0.6}Al_{0.4}As/GaAs$	Ref. 33
5	$Ga_{0.5}Al_{0.5}As/GaAs$	LPE
6	$Ga_{0.18}Al_{0.82}As/GaAs$	LPE
7	$Ga_{0.1}Al_{0.9}As/GaAs$	LPE
8	$Ga_{0.1}Al_{0.9}As/GAAs$	LPE
9	$Ga_{0.47}In_{0.53}As/InP$	MOCVD
10	$Ga_{0.47}In_{0.53}As/InP$	LPE
11	$Ga_{0.47}In_{0.53}As/InP$	MOCVD
12	$Ga_{0.47}In_{0.53}As/InP$	MBE
13	$Ga_{0.47}In_{0.53}As/InP$	MBE

InAs-like mode is not observed[32]. The characteristics of the samples are given in Table II. For sample #1 the LO_1 - mode was too weak to be observed. For sample # 4 no data on the LO_1 peak was reported. The lineshape of the LO_2 mode for samples #6, #7 and #8 was complicated by the presence of the AL feature (see Fig. 9) and so no meaningful data could be deduced.

The agreement is quite good between the experimental points and the theoretical curve in Fig. 10. This demonstrates that it is possible to evaluate a microscopic spatial coherence length, L, over which the material is compositionally ordered.

The data in Fig. 10 reveals several very interesting features. For example for $Ga_{1-x}Al_xAs$ for the Ga-rich samples the GaAs-like mode is relatively narrow and symmetric in relation to the AlAs-like mode (for example, samples #2 and #3). However, this situation is reversed at $x > 0.5$, i.e. the AlAs-like mode becomes narrower and more symmetric than the GaAs-like feature. This effect is related to the difference in SC length for the GaAs - and AlAs - sublattices as a function of composition x. Barker et.al.[30] have also reported the narrowing of the linewidth of the GaAs-like phonon when the sample composition is rich in Ga and narrowing of the AlAs-like feature for high Al concentrations.

Jusserand and Sapriel also have explored the relation between alloy-induced q-vector relaxation and the asymmetry of the LO-phonon mode[33]. Their model differs from that of Ref. 31 in several important features: (a) for convenience they used a Lorenztian to describe the q-vector distribution, (b) their integral is one-dimensional in q-space (dq instead of d^3q), (c) a composition dependent broadening $\Gamma_o(x)$ and (d) a quadratic dispersion is used which is not valid over the entire BZ. Also Ref. 33 fits the asymmetry of only the GaAs-like mode (to $x = 0.5$) and not the AlAs-like feature. Thus the model of Ref. 31 is much more general and the results are more comprehensive.

Also, recently some extremely interesting Raman experiments [34,35] have been reported on the metastable semiconducting alloys $(GaAs)_{1-x}Ge_x$ and $(GaSb)_{1-x}Ge_x$. The Raman spectra from the former crystalline alloy exhibits a "single-mode" type behavior i.e., only one set of optic modes[34]. The degenerate optic mode of Ge decreased in frequency and split into two GaAs-like modes with the addition of less than 10 mole % GaAs. With further increases in GaAs concentration the higher-frequency mode remained with the longitudinal optic mode of GaAs (at about 292 cm^{-1}) while the lower frequency mode broadened, decreased in frequency more rapidly and finally merged with the TO mode of GaAs at 269 cm^{-1}. The authors suggest that this highly non-linear behavior may be due to a template effect with the GaAs substrate.

For the crystalline $(GeSb)_{1-x}Ge_x$ system optic phonons exhibit a "one-two" type mode behavior, i.e., two sets of optic modes are observed over part of the composition range with only one mode seen over the remaining range of compositions[35]. These results are shown in Fig. 11. According to the usual Raman selection rules, for the <100> backscattering configuration the GaSb LO mode and the Ge optic mode are

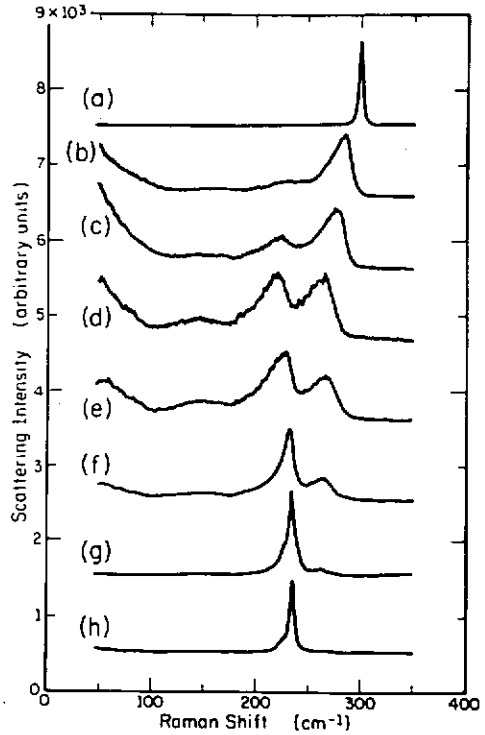

Fig. 11 Raman spectra from single crystals
(a) Ge
(b) $(GaSb)_{0.27}Ge_{0.73}$
(c) $(GaSb)_{0.44}Ge_{0.56}$
(d) $(GaSb)_{0.66}Ge_{0.34}$
(e) $(GaSb)_{0.76}Ge_{0.24}$
(f) $(GaSb)_{0.86}Ge_{0.14}$
(g) $(GaSb)_{0.94}Ge_{0.06}$
(h) (GaSb) (Ref. 35)

allowed, but the GaSb TO mode is forbidden. Figure 11 shows that two optic modes were observed in the alloy spectra, one near the GaSb LO mode at 234 cm^{-1} and one near the Ge optic mode at 300 cm^{-1}. The GaSb-like mode does not shift appreciable in frequency as the GaSb content is decreased; however, its intensity falls rapidly and the peak broadens considerably so that it was just discernable in the $(GaSb)_{0.27}Ge_{0.73}$ spectra. On the other hand, the frequency of the Ge-like mode decreased from 300 to 257 cm^{-1} and the intensity decreased in an approximately linear fashion as the Ge concentration was decreased from 100 to 6 mole %. The linewidth of this mode remained almost constant in the alloys. The strong damping of the GaSb-like mode with decreasing GaSb concentration suggests that $(GaSb)_{1-x}Ge_x$ follows an intermediate one-two mode pattern. In two-mode behavior, the optical modes of the pure crystal end-members evolve into a localized impurity mode of that constituent in the other end-member. Intermediate behavior occurs when creation of a distinct localized mode does not take place. In this alloy, it is suggested that small concentrations of Ga and Sb in Ge do not induce localized modes in the lattice for the following reasons: (1) Ga has too small a mass difference with Ge to significantly perturb the lattice, and (2) the Ge crystal does not have a gap in its phonon density of states for creation of the gap mode associated with heavy substitutional Sb impurities (M_{SB}/M_{Ge} = 1.69). Spectra taken from a 99.8 mole % Ge sample showed no evidence for Ga or Sb related local modes. In contrast, at the other end of the alloy concentration range, the Ge-like mode merged into a local mode of 257 cm^{-1} as shown in Fig. 11 (g). The authors attribute this to Ge atoms residing on Sb sites. Ge atoms on Ga sites have too small a mass difference for creation of a gap mole.

Note that in Fig. 11 the lineshape of the Raman spectra from the alloy material is asymmetry broadened in relation to the end point materials. These authors also attribute this effect as the q-vector relaxation associated with the alloy disorder[35]. It would be of considerable interest to analyze the alloy Raman lineshapes of Fig. 11 on a more detailed basis similar to that presented above for the $Ga_{1-x}Al_xAs$ and $Ga_{0.47}In_{0.53}As$ materials (see Fig. 10).

Reference 35 also makes an interesting observation with regard to the polarization dependence of the alloy modes, i.e., in spite of the substitutional disorder in these crystalline samples the polarization dependence of the optic modes was the same as that of the zone-center modes observed in pure GaSb and Ge. Note that in Fig. 5a for a fluence of 2.4 x $10^{13}cm^{-2}$, which corresponds to a spatial correlation length of about 45 Å, the LO phonon of the ion-damaged material also obeys the appropriate polarization selection rules.

Compositional (or structural) disorder can also actuate normally forbidden Raman features such as zone-boundry modes. For example, the structure at about 150 cm^{-1} in Fig. 11 has been attributed to a zone-edge acoustic mode induced by the alloy disorder. Note that as shown in Fig. 5a, structural disorder can also induce zone-edge features. The use of disorder-actuated longitudinal acoustic (DALA) and transverse acoustic (DATA) modes for materials characterization is presented in Refs. 4 and 30. The relation between the DATA feature and second-order Raman scattering is discussed in the next section.

Second-order Raman effects While most of the attention in Raman scattering has been devoted to the description and understanding of the properties of the first-order Raman features of elemental, binary and alloy semiconductors much less effort has been spent on studying two-phonon spectra, where the density of states favors near-zone edge phonons (ZEP) e.g., the X and L points in Figs. 1a and 1b.

Recently two works have utilized the properties of the two-phonon Raman spectra for alloy semiconductor characterization. Teicher et. al. have investigated the two-phonon spectra of $Ga_{1-x}Al_xAs$ and $GaP_{1-x}As_x$[36] while Sapriel et. al.[37] have gained information about the crystalline quality of the GaAs layers of GaAs-$Ga_{1-x}Al_xAs$ superlattices by comparing the disorder-activated transverse-acoustic (DATA) modes and the second-order Raman lines.

Reference 36 reports that the two-phonon spectra show coupled zone-edge phonons, which are GaAs-like,

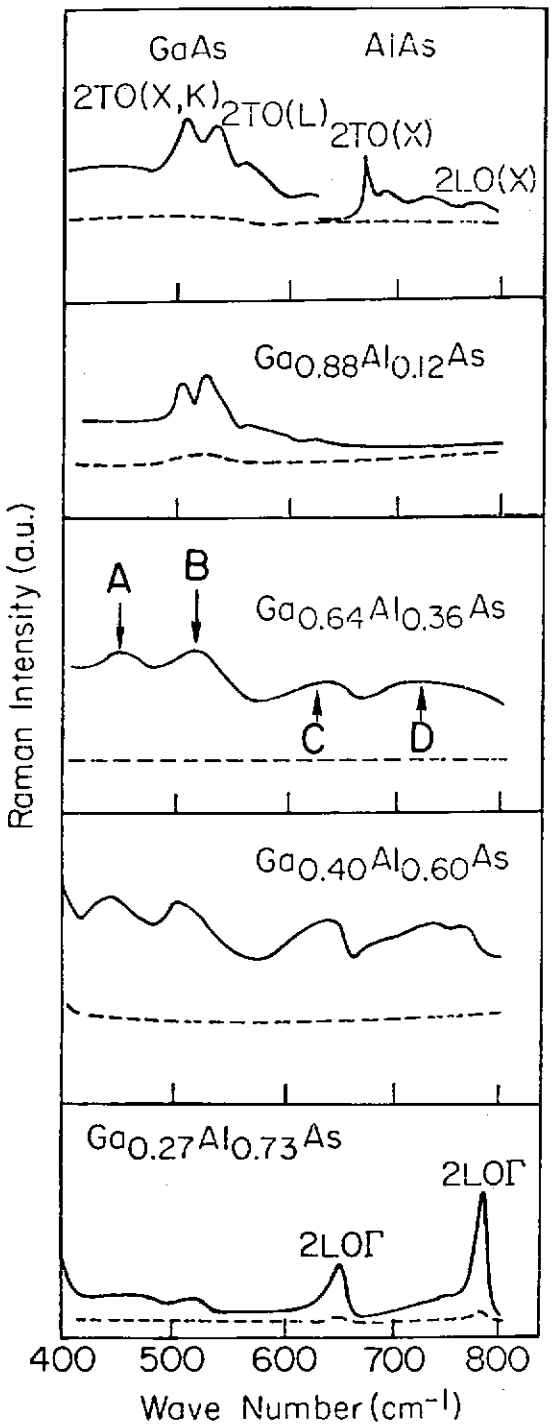

Fig. 12 Second-order Raman spectra of GaAs, AlAs, $Ga_{0.88}Al_{0.12}As$, $Ga_{0.64}Al_{0.36}As$, $Ga_{0.40}Al_{0.60}As$ and $Ga_{0.27}Al_{0.73}As$ (Ref.36).

AlAs-like and also combinations of GaAs-like and AlAs-like zone-edge phonons. Figure 12 shows the two-phonon RS of several $Ga_{1-x}Al_xAs$ crystals together with the spectra of GaAs and AlAs. As long as the aluminum content is small ($x < 30\%$) the two-phonon spectrum is very much like that of GaAs, the peaks tending to blur with increasing x. The intensity of the two-phonon spectrum normalized to that of LO_1, remains roughly constant. When x = 36.5% the two-phonon RS is composed of four bands; the A band 420 $cm^{-1} < \omega < 480\ cm^{-1}$, the B band 480 $cm^{-1} < \omega < 560\ cm^{-1}$ the C band 560 $cm^{-1} < \omega < 670\ cm^{-1}$, and the D band 670 $cm^{-1} < \omega < 800\ cm^{-1}$. The B band is GaAs-like but without the structure seen in the pure material. The D band is AlAs-like, but the sharp 2TO (X,K) peak has disappeared. In addition to these two bands, which are found in any two-mode-behavior-mixed crystals, two additional bands are seen. The one labelled as C between the GaAs-like and the AlAs-like two phonon bands is clearly due to combinations of GaAs and AlAs optical ZEP. Prior to this report such a combination band has not been seen in any non-resonant two-mode-behavior-mixed-crystal. The A band, which does not appear in GaAs is due to combinations of acoustical and optical phonons of GaAs and AlAs. The intensity of the B band, normalized to the LO one, does not vary with "x". For x = 60% the spectrum is similar to that of $Ga_{0.73}Al_{0.27}As$, with the four bands clearly defined. For $GaP_{1-x}As_x$ the A and C bands discussed above are not seen, i.e., only ZEP associated with the GaP and GaAs modes.

These results have been qualitatively explained by assuming a random distribution of Ga and Al atoms in the $Ga_{1-x}Al_xAs$ crystals and a distortion of the lattice structure as well as a departure from a random distribution of atoms(i.e., clustering) in the $GaP_{1-x}As_x$system.

Sapriel et. al. have studied Raman and Brillouin scattering from GaAs-$Ga_{1-x}Al_xAs$ superlattices and have observed zone-folding of the LA branch. In addition they have investigated the relative intensities of the disorder-activated transverse acoustic (DATA) mode and the second-order 2TA mode in GaAs from the zone edge of the unfolded BZ[37]. Since the amplitude of the DATA mode is clearly less than that of the 2TA structure they conclude that the disorder in the GaAs layers is quite small. The good crystalline quality of the superlattices have also been verified by the high degree of polarization of the Raman features[37].

$Hg_{1-x}Cd_xTe$ and CdTe

Despite the significance of $Hg_{1-x}Cd_xTe$ from both fundamental and applied perspectives and the utility of RS in studying semiconductors only two Raman investigations of bulk (or thin film) material have been reported[38,39]. Mooradian and Harman[38] have used RS to measure the composition dependence of the transverse (TO) and longitudinal (LO) optical phonon frequencies. $Hg_{1-x}Cd_xTe$ has a two-mode behavior like $Ga_{1-x}Al_xAs$. Even though the spectra for the constituent binaries, HgTe and CdTe, were presented, no spectrum for $Hg_{1-x}Cd_xTe$ was included in the paper. Furthermore, the polarization dependence of the various features was not investigated. The compositional dependence of the To and LO frequencies has also been investigated using far infrared reflectivity (FIR)[40,41].

Recently, the first polarization-dependent RS study in $Hg_{1-x}Cd_xTe$ ($x \approx 0.2$) has been reported[39]. The

experiment was performed at 77°K in the backscattering geometry from both < 100 > and < 111 > surfaces with various polarization configurations and using several excitation wavelengths near resonance with the E_1 optical gap. The bulk HgTe-like and CdTe-like TO and LO phonon (q=0) features were observed as well as a strong symmetry forbidden TO mode (HgTe-like) from the < 100 > surface. In addition, features were recorded which appear to be related to deviations from the ideal, stoichiometric crystal. For example, a feature at 108 cm^{-1} was reported which has also been seen in HgTe but not CdTe. It has been suggested that it may be due to an anti-site defect, i.e., Hg on Te sites. In addition another structure has been tentatively assigned to clustering effects which have also been observed in FIR measurements[41].

Reference 39 also reports the observation of a coupled LO phonon-intersubband excitation (S_-) due to the inversion layer (which occurs in p-$Hg_{1-x}Cd_xTe$). This S_- feature was found to be extremely sensitive to surface treatment and may prove to be a valuable tool to study surface conditions and preparation. It has been found that this feature is more surface sensitive than electrolyte electroreflectance[39] at the E_1 optical feature since the penetration depth of the light is about 250 Å in this wave length region while the depth of the inversion layer is $\lesssim$ 50 Å.

As reviewed by G. Schwartz[6] RS can be utilized to study the nature of oxides on the surface of various compound semiconductors. Recently, Adar et. al.[42] have measured RS from native oxide films on $Hg_{0.7}Cd_{0.3}Te$. They have observed features which can be correlated with the Raman peaks of bulk $HgTeO_3$, $CdTeO_3$ and TeO_2. Their spectra below 200 cm^{-1} contains spurious effects from nitrogen in the air.

The use of Raman microprobe spectroscopy to characterize Te precipitates in Bridgmann-grown CdTe crystals has been reported[43]. These precipitates appear to be in the high pressure phase since the observed spectral lines are similar to those of elemental Te under high pressure.

Conduction band masses and scattering times

Olego et. al., have recently reported the determination of the compostion dependence of the electron effective mass (and scattering times) for the $In_{1-x-y}Ga_xAl_yAs$ (lattice matched to InP) by means of Raman scattering from the coupled LO-phonon-plasma mode[44]. As discussed in Ref. 1-4, the peak of the plasmon-like Raman band (L_+) is a measure of the plasma frequency ω_p (provided it lies well above the LO phonon frequencies) while the linewidth gives a scattering time. Since the plasma frequency ω_p is related to the carrier effective mass $m_c^*(\omega_p^2 \alpha 1/m_c^*)$ by measuring the position (and width) of the plasmon-like mode as a function of composition these authors were able to deduce the mass (corrected for non-parabolic effects) as well as the scattering time, and hence mobilities.

Superlattices and quantum well structures

There is a considerable body of work on Raman scattering from superlattices[4,30,37,45] and quantum well structures. Most of these works have been devoted to the investigation of basic interactions, such as light scattering from the two-dimensional electron gas confined in modulated doped structures[46-48] etc. While these studies are of considerable fundamental importance, it appears that only two areas have specific characterization applications. These are discussed below.

Zone-folding effects - In a superlattice the new periodicity in the direction perpendicular to the layers result in a folding of the Brillouin zone[49]. Two recent studies have shown clear RS evidence for zone-folded acoustic phonons in a superlattice[37,45]. Shown in Fig. 13 is the Raman spectru, of a superlattice consisting of 1720 periods of 13.6 Å GaAs-11.4 Å AlAs grown on a < 100 > GaAs substrate[45]. The sharp features denoted $A_1^{(1)}$ and $B_2^{(1)}$ at about 65 cm^{-1} are from LA phonons (see Fig. 1b) folded to the zone center from $q=2\pi/d$ in the extended zone, where d is the superlattice period. Sapriel et. al.[37] have observed similar effects. However, their zone folded LA lines were observed at about 200 cm^{-1} since their superlattice had d = 54 Å. Thus the positions of these lines can be used as a measure of the superlattice period. Although not discussed in the above references the width of these zone-folded lines also may be of value in determining superlattice quality. For example, a broadening of these lines may indicate non-uniform layers.

Quantum well structures - Recently, Pinczuk et. al. have reported the first indication that resonant inelastic light scattering can play a role in the characterization of the transport properties of electrons confined in the GaAs-(AlGa)As heterostructures[48]. An unusual manifestation of the relation of electron mobilities with light scattering spectra is that, particularly for mobilities lower than 30,000 cm^2/Vs, the spectral lines shapes depend on the incident phonon energy. This effect has been interpreted as arising from a breakdown of the requirement of wave vector conservation in resonant inelastic light scattering. Such a breakdown is believed to be associated with electron relaxation processes similar to those that limit the electron mobilities.

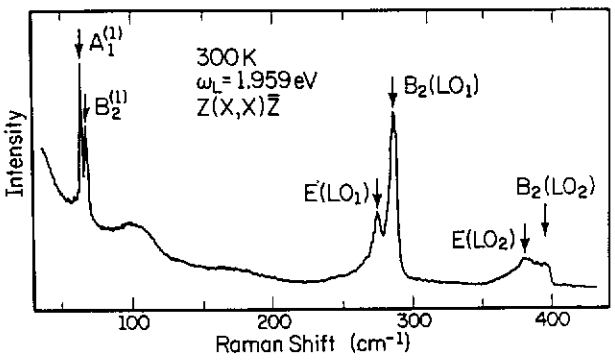

Fig. 13 Raman spectrum of a (GaAs, AlAs) superlattice (Ref. 45).

Figure 14 shows the FWHM of the band of the E_{01} transition of single GaAs-$(Al_{0.12}Ga_{0.88})As$ quantum as well samples with the highest mobilities. These are 28,000 cm^2/Vs, 62,000 cm^2/Vs and 93,000 cm^2/Vs for samples 1, 2 and 3, respectively. Although a correlation between FWHM and electron mobilities could be anticipated, the data in Fig. 14 show that the FWHM measured in sample 1 has an unexpected dependence on the incident photon energy. In this sample, the one of those considered in Fig. 14 that has the lowest mobility, the FWHM has a peak for spectra obtained with photon energies close to the maximum in resonant enchancement (indicated as E_R in Fig. 14).

To interpret these results, these authors have proposed that resonant inelastic light scattering by the intersubband excitations is affected by wave vector relaxation processes similar to those that limit the electron mobilities. These relaxation processes are due to the scattering of the electrons by the Coulomb potential of the ionized donors. Under these circumstances, it is expected that the condition of wave vector conservation breaks down for resonant light scattering. Therefore, the intersubband transitions active in backscattering spectra are no longer necessarily vertical, but may occur with an in-plane wave vector transfer q. The energy of such a non-vertical intersubband transition is shifted from the vertical subband spacing by $\pm\hbar^2/q\cdot\kappa/m^* + \hbar^2q^2/2m^*$, where κ is an arbitrar two-dimensional electron wave vector limited to $|\kappa| < K_F$ and K_F is the Fermi wave vector. Since there is a continuum of such energies, the spectral bands of non-vertical intersubband transitions are expected to show considerable width or even appear as a quasi-continuum.

Thus, in resonant inelastic light scattering spectra of very high mobility electrons in modulated-doped multiple quantum-well GaAs-(AlGa)As heterostructures a correlation between the FWHM of intersubband transitions and the Hall mobilities has been observed.

Interfaces

Semiconductor - vacuum

Among various types of interfaces, the most fundamental one is the interface between a semiconductor surface and vacuum. The surface pinning of the Fermi level originally treated by Mead and Spitzer[50] has been clarified by recent studies in photoemission[51] which showed that on a clean and well-cleaved surface GaAs there are no filled surface states in the gap and consequently no surface band bending. However, exposing the surface oxygen definitely results in a band bending. Stolz and Abstreiter[52] were able to utilize the coupled phonon-plasmon modes in Raman measurements to examine a clean, UHV-cleaved < 110 > GaAs surface. Since the selection rules for backscattering geometry on a < 110 > surface allow pnly first order Raman scattering by transverse optical (TO) phonons (see Table I) and thus the LO-phonon scattering is forbidden by

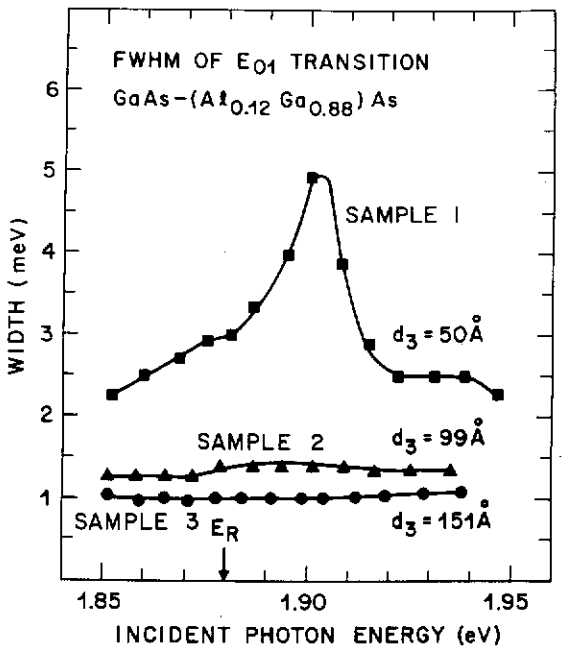

Fig. 14 Full width at half maxima (FWHM) of the E_{01} intersubband transition as a function of incident photon energy. E_R = 1.880 eV is the photon energy of the maximum in resonant enhancement (Ref. 48).

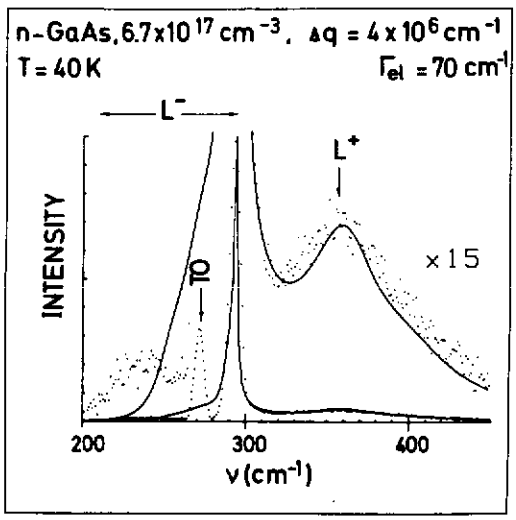

Fig. 15. Coupled LO-phonon-plasmon modes for UHV-cleaved <110> GaAs. Dots: experimental data for λ_ℓ =406.7 nm $z(yy)\bar{z}$: Full line: fit with Lindhard-Mermin dielectric function (TO phonon not included by fit). (Ref. 52).

symmetry. Under resonant Raman conditions near the E_1 peak of GaAs at 2.94 eV, the breakdown of this symmetry forbidden scattering is quite pronounced due to surface electric field, and other impurity induced effects. Figure 15 shows an example of their results for a UHV-cleaved < 110 > oriented n-GaAs having a carrier concentration of 6.7×10^{17} cm^{-3}. As carrier concentration increases, optical absorption increase confines the incident laser light closer to the surface resulting in larger scattering from the forbidden LO due to stronger effects from the surface electric field[11,46]. Since the intensity of the allowed TO phonon is unaffected by the surface charge, the ratio I_{LO}/I_{TO} may serve to quantity the effects of the surface electric field as a function of the carrier concentration, and in turn may serve to quantify the flat band condition. Returning to Fig. 15 note that there is present a strong LO peak obviously uncoupled to the plasmon mode. Offhand, one would have concluded that a fairly sizable surface depletion still existed. However, Stolz and Abstreiter reasoned that a very large optical absorption in the order of 10^6 cm^{-1} which is in the range or larger than the Thomas-Fermi screening vector causing the plasmon to be heavily Landau damped[46,52] and thereby causing the LO-mode to be unscreened. From the phonon dispersion of GaAs, and unscreened LO-peak corresponding to $\Delta q \approx 4 \times 10^6$ cm^{-1} should be down shifted in frequency by 1 cm^{-1} (see Fig. 7). Since this shift depends on optical absorption, which in turn increases with carrier concentration, the higher the carrier density, the greater should be this shift. We suggest further work at this point.

Schottky barrier and MOS junctions

As pointed out by Pinczuk et. al.[54] not only can Raman scattering be used, as in photoemission, to study band bending on clean surfaces, it can also provide information for heavily contaminated surfaces. Schottky barriers made with semitransparent metal films as well as heterojunctions in which one of the layers is at least partially transparent to the incident light. The above authors observed that the band bending at the etched < 111 > B surface of n-InP is approximately 0.2 V, much below 0.55 V after evaporation of a partially transparent Ag film due to the formation of a Schottky barrier. Furthermore the difference in band bending obtained for a low and a high power level should be equal to the saturation surface photovoltage. Thus Raman scattering is a useful tool for the study of band bending in Schottky barrier formation and effects related to surface photovoltage.

The Raman scattering from heavily doped n-GaAs with and without a semi-transparent metal film has been investigated by Tsu et. al.[55]. They have reported a shift of the LO phonon frequency from 292 cm^{-1} to as high as 302 cm^{-1} depending on the applied bias voltage. They speculated that the presence of a metal contact may increase the surface recombination time of the laser excited carriers resulting in a shift to higher frequency due to plasmon-phonon coupling. Although a systematic study on the intensity dependence was not pursued in their work, it seems that such as investigation can further clarify the mechanism as well as the possible application to the field of surface recombination and steady state carrier injection.

Several groups have recetnly used Raman scattering to probe reactions at the metal/semiconductor interface. Nemanich et. al. have studied the interfacial structure of Pd on < 100 > Si[56] as well as Pd on a-Si:H[57] while Tsang et. al. have investigated Pt on < 100 > and < 111 > Si surfaces[58]. Both groups report new Raman features in the range 50 - 300 cm^{-1} which can be assigned to the formation of the silicide. For example, vibrational modes of surface silicide layers as thin as 10 Å and silicide layers less than 40 Å thick buried under 140 Å of Pt have been observed[58]. These works are of considerable significance and demonstrate the utility of Raman spectroscopy for silicide interface studies to identify and characterize thin reacted layers. In particular the use of the interference phenomena to enhance the Raman signal from the interfacial region is similar to the quarter-wave transfer for impedance matching.

Raman scattering at resonance at the E_1 gap at InAs surfaces in MOS junctions formed on n- and p-InAs substrates has been used to obtain information about the space-charge region. A narrow peak just below the unscreened LO phonon peak for both n- and p-InAs at 77°K for zero and positive gate voltages was observed by Ching et. al.[59]. It has been attributed to scattering by LO phonons coupled to collective inter-subband excitations which is the couterpart of the coupled plasmon-phonon mode in a two-dimensional electron-plasmon system. Since the electron wavefunction in either an accumulated or inverted surface region is highly localized, there will be broadening associated with the q-vector relaxation and down shifts due to dispersion because the maximum phonon frequency in most diamond and zinc-blende semiconductors is located at q = 0. A specific theoretical treatment of Raman scattering in surface quantization has been explored by Tsu and Esaki[60]. On the other hand, this wavevector relaxation due to wavefunction localization is a particular case of a general class of wavevector relaxation treated in this review.

Heterojunctions

Raman scattering may be used to characterize the interface of a heterojunction formed by a GaAlAs epilayer on GaAs substrate[61]. In particular, information can be obtained about (a) composition x of the $Ga_{1-x}Al_xAs$ epilaer, (b) crystalline quality of the epilayer, (c) band bending at the interface, (d) carrier depletion from the GaAs substrate, and (e) carrier concentration of the GaAs substrate material. Figure 16 shows the Raman spectra of GaAs substrate and that of GaAlAs epilayer taken from Parayanthal et. al.[59-61]. Note that the L_- and L_+ modes of the substrate were also detected because the optical absorption for the epilayer at 5145 Å is quite small. The position of the L_- is down shifted somewhat from the GaAs substrate shown in the top spectrum. This is an indication that a slight carrier depletion has resulted in the formation of the heterojunction. In fact, the presence of a potential mismatch at a GaAlAs-GaAs interface was first experimentally confirmed by tunneling experiment[62] in a double barrier, GaAlAs-GaAs-GaAlAs structure. Because of the potential mismatch, it is obvious that band bending will result and subsequently lead to a slight carrier

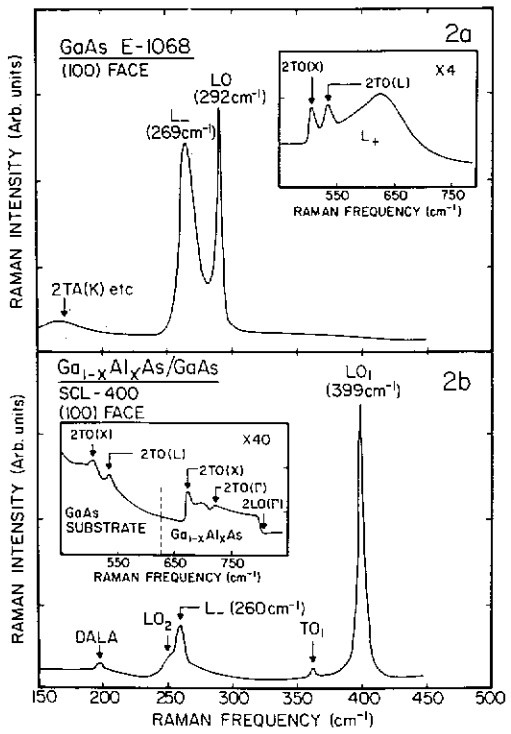

Fig. 16 Raman spectrum of GaAs E-1068, the substrate used in growing the $Ga_{1-x}Al_xAs$ epilayer of sample SCL-400. The upper - hand corner shows the coupled mode L_+. The sharper structures are due to second-order two-phonon Raman scattering. (b) Raman spectrum of $Ga_{1-x}Al_xAs$/GaAs sample SCL-400. The upper left-hand corner shows the Raman spectrum in the range 500 - 800 cm^{-1}. The features to the left of the vertical dashed line are from the GaAs substrate and those to the right are from $Ga_{1-x}Al_xAs$ epilayer. (Ref. 60).

depletion. However, the interfacial region is graded in a LPE grown heterostructure having a linear length comparable or exceeding the depletion width, therefore interdiffusion of dopants should be involved. In fact, since the GaAs substrate is doped with Si at 3 x 10^{18} cm^{-3} and the LPE melt is not doped with Si, the dopant is expected to outdiffuse from the GaAs into the LPE melt. Similarly, Te in the melt would result in a doping at the GaAs surface layer is lower than the bulk. They have estimated the doping level in the epilayer to be n = 1.2 x 10^{18} cm^{-3}. This type of interdiffusion and its effect on carrier concentration and of course, the information whether band bending is present, can be obtained from one scan using Raman spectroscopy. The value of Raman scattering in the characterization of the interfacial region of a heterojunction is quite conclusive.

Strain

The Raman spectrum is sensitive to the strain in the lattice and therefore can be used to measure stress in crystalline samples. Under stress, there are changes in the spring constants which characterize the phonon dispersion of solids. Many detailed studies of the effects of uniaxial and hydrostatic pressure on the frequency of the zone-center optical phonons by Raman scattering have appeared in the literature. In particular, Anastassakis et. al.[63] experimentally obtained the splitting and shifts of the q = 0 triply degenerate optical phonons for a uniaxial stress along < 001 > or < 111 > of crystalline silicon, and Cerdeira et. al.[64] have extended the study to include Ge as well as many zinc-blende semiconductors. Strain-induced shifts of zone edge phonons have been measured by Weinstein and Piermarini[65]. These investigators[62-64] obtained the phenomenological coefficients which describe the change in spring constant due to an applied strain. These values are now central to the detailed analysis of the interfacial strain effects discussed below.

Raman spectroscopy has been used by a number of investigators to study stress effects in Si/SiO_2 or Si/Al_2O_3 interfaces[66-70]. The method is direct, non-destructive and can be applied at various temperatures. For example, Englert, Abstreiter and Pontcharra determined the built-in stress in silicon on sapphire devices[66] using the result of Ref. 63. It was found that epitaxially grown silicon films having an orientation < 001 > on < 1012 > sapphire substrate develop a built-in stress of 7 kbar at room temperature. Shown in Fig. 17 are their results. The origin of this stress is the differential thermal expansion coefficient between silicon and sapphire. Since the epitaxial growth is usually at temperatures above 750°C, on cooling, the larger thermal expansion of sapphire results in a two-dimensional compressional stress in silicon. Recently, the Raman microprobe technique has been used to map the local stresses in patterned islands of laser-crystallized silicon on bulk glass[71] and on a laser-crystallized, seeded lateral epitaxial silicon film on an oxidized silicon wafer[72]. It was found in Ref. 71 that a stress increased from 2 kbar in the seed region to 5 kbar in the silicon-on-insulation region at distances greater than 20 μm from the seed-silicon-on-insulation boundary. Depth variations of the stress may be obtained by using different wavelengths of the exciting laser lines. This type of Raman measurements adds a new dimension to the study of grain boundary formation.

Another unique application of Raman scattering for the study of microadhesion has been recently introduced by Gonzalez-Hernandez, Martin and Tsu[73]. The techniques involves the correlation of the measured Raman shift of the zone-center optical phonon frequency with the differential thermal expansion coefficient between the silicon film and the substrate material. It was observed for example that silicon films, whether epitaxially grown or microcrystalline form may or may not show a shift corresponding to the values compatible with thermal expansion dependent upon the degree of microadhesion. Furthermore, amorphous silicon when crystallized, the stress-free condition is reached always at the crystallization temperature regardless of the

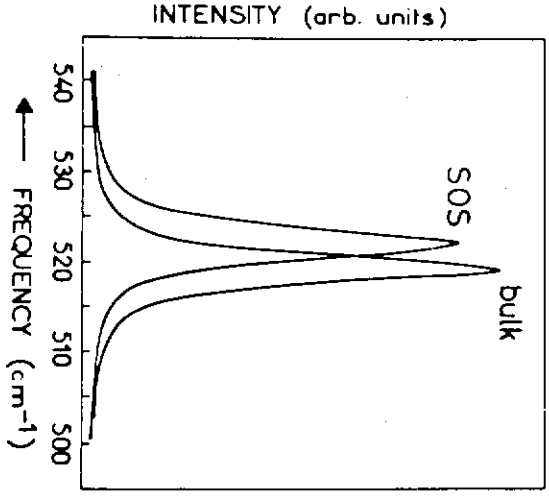

Fig. 17. Raman spectra of bulk silicon and silicon on sapphire (SOS). The shift is due to built-in stress in the silicon film (Ref. 66).

annealing temperature. This work is described further in the following article.

These are the powerful outgrowths of fundamental physics, the phonon frequency shift due to stress, to areas of technology.

Conclusion

We have reviewed a number of recent developments which demonstrate that Raman scattering is a powerful tool for characterizing semiconductors in bulk, thin films or device form. The sensitivity of this spectroscopic method to local environment, the second-order nature of the interaction process, the coupling to various excitations such as plasmons and its response to external perturbations such as electric fields and strain make it an extremely versatile tool. Thus Raman scattering can be used to obtain valuable information about many materials or device parameters such as crystal quality (including finite size effects, structural and/or topological disorder), composition of alloy semiconductors, carrier concentration scattering processes, interface properties, strains, etc. Therefore, we strongly suggest that Raman spectroscopy become a standard laboratory tool for semiconductor characterization.

Acknowledgements

F. H. Pollak wishes to thank the IBM Support for University Research (SUR) Program for its support of portions of this work. R. Tsu acknowledges sponsorship from The Standard Oil Company (Ohio).

References

1. See, for example, Scattering of Light by Crystals, by Hayes, W. and Loudon, R., John Wiley and Sons, 1978.
2. See, for example, Light Scattering in Solids, Vol. 1, Springer-Verlag, 1975.
3. Abstreiter, G., Bauser, E., Fischer, A. and Ploog, K., Appl. Phys. , Vol 16, p.345, 1978.
4. Tsu, R., SPIE Proceedings, Vol. 276, p. 78, 1981.
5. Tsu, R., in Defects in Semiconductors, North Holland, p. 445, 1981.
6. Schwartz, G. P., SPIE Proceedings, Vol. 276 p. 72, 1981.
7. For a discussion of Raman scattering from other excitations such as electrons see Ref. 1 and Klein, M. V. in Ref. 2.
8. Shuker, R. and Gammon, R. W., Phys. Rev. Lett., Vol. 25, p. 222, 1970.
9. Most semiconductors are opaque in the wavelength region of commonly used lasers such as Ar^+ or Kr^+ (i.e., visible or near-visible)and hence the backscattering geometry must be employed.
10. See, for example, Anastassakis, E. M. in Morphic Effects in Lattice Dynamics, North-Holland, p. 158, 1980.
11. Rubloff, G. W., Anastassakis, E. and Pollak, F. H., Solid State Comm., Vol. 13, p. 1755, 1973.
12. Tsu, R., Gonzalez-Hernandez, J., Doehler, J. and Ovshinsky, S. R., Solid State Comm., Vol. 46, p. 79, 1983.
13. See, for example, Richter, H., Wang, Z. P. and Ley, L., Solid State Comm., Vol. 39, p. 625, 1981 and references therein.
14. Hayashi, S. and Kanamori, H., Physica, Vol. 117B and 118B, p. 520, 1983.

15. Tsu, R., Chao, S. S., Izu, M., Ovshinsky, S. R., Jan, G. J. and Pollak, F. H., J. de Physique , Vol. 42, p. 269, 1981.

16. Gonzalez-Hernandez, J. and Tsu, R., Appl. Phys. Lett., Vol. 42, p. 90 (1983).

17. Tsu, R., Gonzalez-Hernandez, J., Chao, S. S., Lee, S. C. and Tanaka, K., Appl. Phys. Lett., Vol. 40 p. 534 (1982).

18. Maley, N., Pilione, L. J., Kshirsagar, S. T. and Lannin, J. J., Physics, Vol. 117B and 118B, p. 880 (1983).

19. Shimada, T., Katagama, Y., Nakagawa, K., Matsubara, H., Migiraka, M. and Maruyama, E., to be published in the Proc. 10th Int. Conf. on Amorphous and Liquid Semiconductors, Tokyo, 1983.

20. Wada, N., Gaczi, P. J. and Solin, S. A., J. Non-Cryst. Solids, Vols.15 and 16, p. 543 (1980); Solin, S.A., Wade, N. and Wong, J., Inst. Phys. Conf. Ser., Vol. 43, p. 721 (1979).

21. Dillon, R. D., Khan, A. Axim, Ullman, F. G., Hardy, J. R., Katbanant, V., Woollam, J. A. and Banks, B., Bull. Am. Phys. Soc., Vol. 28, p. 563 (1983); ibid, submitted to Phys. Rev.

22. Kampas, F. J. and Pollak, F. H., Bull. Am. Phys. Soc., Vol. 28, p. 565 (1983).

23. Tsu, R., Gonzalez-Hernandez, J. and Pollak, F. H., submitted to Phys. Rev. Letts.

24. Tsu, R., Gonzalez-Hernandez, J., Hernandez-Calderon, I. and Luengo, C. A., Solid State Comm., Vol. 24, p. 809, 1977; Tsu, R., Gonzalez-Hernandez, J. and Hernandez-Calderon, I., Solid State Comm., Vol. 27, p. 507, 1978.

25. See, for example, Tiong, K. K., Amirtharaj, P. M., Pollak, F. H. and Aspnes,D. E., to be published in Appl. Phys. Letts. and references therein.

26. See, for example, Meyers, D. R., Gourley, P. L. and Peercy, P. S., to be published in J. Appl. Physics, Meyers, D. R., and Gourley, P. L., J. Electrochem. Soc., Vol. 130, p. 217 (1983) and references therein.

27. Aspnes, D. E., Kelso, S. M., Olson, C. G. and Lynch, D. W., Phys. Rev. Letts., Vol. 48, p. 1863 (1982).

28. Nakamura, T. and Katoda, T., J. Appl. Phys., Vol. 8, p. 5870 (1982).

29. Barker, A. S. and Sievers, A. J., Rev. Mod. Phys., Vol. 47, p. S2, 1975 and references therein.

30. Barker, Jr., A. S., Merz, J. L., and Gossard, A. C., Phys. Rev., Vol. B17, p. 3181, 1978.

31. Parayanthal, P. and Pollak, F. H., submietted to Phys. Rev. Letts.

32. Pearsall, T., Carles, R. and Portal, J. C., Appl. Phys. Letts., Vol. 42, p. 436, 1983.

33. Jusserand, B. and Sapriel, J. Phys. Rev., Vol. B24, p. 7194, L981.

34. Barnett, S. A., Ray, M. A., Lastras, A., Kramer, B., Greene, J. E., Raccah, P. M. and Abels, L. L., Electronic Letts., Vol. 18, 891 (1982).

35. Krabach, T. N., Wada, N., Klein, M. V., Cadien, K. C. and Greene, J. E., Solid State Comm., Vol. 45, p. 895, 1983.

36. Teicher, M., Beserman, R., Klein, M. V. and Morkoc, H., submitted to Phys. Rev.

37. Sapriel, J., Michel, J. C., Toledano, J. C., Vocher, R., Kervarec, J. and Regreny, A., Phys. Rev., Vol. B28, p. 2007, 1893.

38. Mooradian, A. and Harman, T. C., Proc. Conf. Physics of Semimetals and Narrow-Gap Semiconductors, Dallas, 1970, Pergammon Press, 1971, p. 297.

39. Amirtharaj, P. M., Tiong, K. K. and Pollak, F. H., J. Vacuum Sci. Technol., Vol. A1(3), p. 1744, 1983.

40. Baars, J. and Sorger, F., Solid State Comm., Vol. 10, p. 875, 1972.

41. Kozyrev, S. P., Vodopyanov, L. K. and Triboulet, R., Solid State Comm., Vol. 45, p. 383, 1983.

42. Adar, F., Kvaas, R. e., and Rhiger, D. R., Proc. 1982 Conf. on Advances in Materials Characterization, Plenum, 1983.

43. Shin, S. H., Bajaj, J., Moudy, L. A. and Cheung, D. T., Appl. Phys. Letts., Vol. 43, p. 68, 1983.

44. Oleg, D., Chang, T. Y., Silberg, E., Daridi, E. A. and Pinczuk, A., Appl. Phys. Letts., Vol. 41, p. 476, 1982.

45. Colvard, C., Merlin, R., Klein, M. V. and Gossard, A. C., Phys. Rev. Letts., Vol. 45, p. 298, 1980.

46. See, for example, Pinczuk, A., Abstreiter, G. and Cardona, M., Light Scattering in Solids, Vol. 4, Springer-Verlag, to be published.

47. Petrou, A. P., Perry, C. H., Smith, M. C., Worlock, J. M., Aggarwal, R. L., Gossard, A. C. and Wiegmann, W., this conference; Kirillov, D. and Merz, J. L., this conference.

48. Pinczuk, A., Worlock, J. M., Stormer, H. L., Gossard, A. C. and Weigmann, W., J. Vac. Sci. Technol., Vol. 19, p. 561, 1981.

49. Tsu, R., and Jha, S. S., App. Phys. Letts., Vol. 20, p. 16, 1972.

50. Mead, C. A. and Spitzer, W. G., Phys. Rev., Vol. 134, p. 713, 1964.

51. Pianetta, P., Lindau, I., Gregory, P. E., Garver, C. M. and Spicer, W. E., Surf. Science, Vol. 72 p. 298, 1978.

52. Stolz, H. J. and Abstreiter, G., J. Vac. Sci. Technol., Vol. 19, p. 380, 1981.

53. Tsu, R., Phys. Rev., Vol. 164, p. 380, 1967.

54. Pinczuk, A., Ballman, A. A., Nahory, R. E., Pollack, M. A. and Worlock, J. M., J. Vac. Sci. Technol., Vol. 16, p. 1168, 1979.

55. Tsu, R., Kawamura, H., and Esaki, L., Solid State Comm., Vol. 15, p. 321, 1974.

56. Tsai, C. C., Nemanich, R. J., and Sigmon, T. W., J. Phys. Soc. Japan, Vol. 49, Suppl. A., p. 1265, 1980.

57. Nemanich, R. J., Tsai, C. C., Thompson, M. J., and Sigmon, T. W., J. Vac. Sci. Technol., Vol. 19, p. 685, 1981.

58. Tsang, J. C., Matz, R., Yokote, Y. and Rubloff, G. W., submitted to J. Vac. Sci. Technol.

59. Ching, L. Y., Burstein, E., Buchner, S. and Wieder, H. H., J. Phys. Soc. Japan, Vol. 49, Suppl. A., p. 951, 1980.

60. Tsu, R. and Esaki, L., Proc. Third Int. Conf. Light Scattering in Solids, Campinas, 1975, Flammarion Sciences, p. 533, 1975.

61. Parayanthal, P., Pollak, F. H. and Woodall, J. M., Appl. Phys. Lett., Vol. 41, p. 961, 1982.

62. Chang, L. L., Esaki, L. and Tsu, R., Appl. Phys. Lett., Vol. 24, p. 593, 1974.

63. Anastassakis, E., Pinczuk, A., Burstein, E., Pollak, F. H. and Cardona, M., Solid State Comm., Vol. 8, p. 133, 1970.

64. Cerdeira, F., Buchenauer, C. J., Pollak, F. H. and Cardona, M., Phys. Rev., Vol. B5, p. 580, 1971.

65. Weinstein, B., and Piermarini, G. J., Phys. Rev., Vol. B12, p. 1172, 1975.

66. Englert, Th., Abstreiter, G. and Pontchara, J., Solid State Electron, Vol. 23, p. 31, 1980.

67. Ohmura, Y., Inoue, T. and Yoshii, T., Solid State Comm., Vol. 37, p. 583, 1981.

68. Tsaur, B.-Y., Fan, J. C. C. and Gass, M. W., Appl. Phys. Letts., Vol. 40, p. 322, 1982; Breuck, S. R. J., Tsaur, B.-Y., Fan, J. C. C., Murphy, D. V., Deutch, T. F. and Silversmith, D. J., Appl. Phys. Lett., Vol. 40, p. 895, 1982.

69. Kobayashi, Y., Nakamura, M. and Suzuki, T., Appl. Phys. Lett., Vol. 40, p. 1040, 1982.

70. Moser, F., and Beserman, R., J. Appl. Phys., Vol. 54, p. 1033, 1983.

71. Lyon, S. A., Nemanich, R. J., Jobuson, N. M. and Biegelsen, D. K., Appl. Phys. Lett., Vol. 40, p. 316, 1982.

72. Zorabedian, P. and Adar, F., Appl. Phys. Lett., Vol. 43, p. 177, 1983.

73. Gonzalez-Hernandez, J. G., Martin, D. and Tsu, R., this conference.